Meteorol Atmos Phys 100, 101–119 (2008)
DOI 10.1007/s00703-008-0298-3
Printed in The Netherlands

Meteorology and Atmospheric Physics

[1] Jiangsu Key Laboratory of Meteorological Disasters, Institute of Atmospheric Science, Nanjing University of Information Science and Technology, Nanjing, P.R. China
[2] Center of Earth Observing and Space Research, College of Science, George Mason University, Fairfax, VA, USA
[3] Laboratory of Numerical Modeling for Atmospheric Sciences and Geophysical Fluid Dynamics, Institute of Atmospheric Physics, Beijing, P.R. China
[4] Guangzhou Institute of Tropical and Marine Meteorology, Guangzhou, P.R. China

Interdecadal variations of East Asian summer monsoon northward propagation and influences on summer precipitation over East China

Z. Jiang[1], S. Yang[2,4,*], J. He[1], J. Li[3], J. Liang[4]

With 12 Figures

Received 20 September 2007; Accepted 23 December 2007
Published online 18 August 2008

Summary

The interdecadal variation of northward propagation of the East Asian Summer Monsoon (EASM) and summer precipitation in East China have been investigated using daily surface rainfall from a dense rain gauge network in China for 1957–2001, National Center for Environmental Prediction/National Center for Atmospheric Research (NCEP/NCAR) reanalysis, European Center for Medium-Range Weather Forecast (ECMWF) reanalysis, and Global Mean Sea Level Pressure Dataset (GMSLP2) from Climatic Research Unit (CRU). Results in general show a consistent agreement on the interdecadal variability of EASM northward propagations. However, it appears that the interdecadal variation is stronger in NCEP than in ECMWF and CRU datasets.

A newly defined normalized precipitation index (NPI), a 5-day running mean rainfall normalized with its standard deviation, clearly depicts the characteristics of summer rainbelt activities in East China in terms of jumps and durations during its northward propagations. The EASM northward propagation shows a prominent interdecadal variation. EASM before late 1970s had a rapid northward advance and a northern edge beyond its normal position. As a result, more summer rainfall occurred for the North China rainy season, Huaihe-River Mei-Yu, and South China Mei-Yu. In contrast, EASM after late 1970s had a slow northward movement and a northern edge located south of its normal position. Less summer precipitation occurred in East China except in Yangtze River basin.

The EASM northernmost position (ENP), northernmost intensity (ENI), and EASM have a complex and good relationship at interdecadal timescales. They have significant influences on interdecadal variation of the large-scale precipitation anomalies in East China.

1. Introduction

The summer precipitation over China is closely related to the northward/southward propagation of the East Asian Summer Monsoon (EASM) and its variations, in terms of movement of the rainbelt, onset and duration of rainy season, and precipitation pattern, as well as drought and flood distributions (Tu and Huang 1944; Tao and

*Current address: Song Yang, I. M. Systems Group, and NOAA/NESDIS/Center for Satellite Applications and Research (STAR), 5200 Auth Road, Camp Springs, MD 2076, USA (E-mail: song.2.yang@noaa.gov)

Correspondence: Zhihong Jiang, Jiangsu Key Laboratory of Meteorological Disasters, Institute of Meteorology, Nanjing University of Information Science and Technology, Nanjing 210044, P.R. China (E-mail: zhjiang@nuist.edu.com)

Chen 1987; Ding 1992, 1994). Tu and Huang (1944) conducted a pioneer study of EASM and its influences on weather and climate over East Asia by analyzing the northward propagation of EASM. Gao and Xu (1962) and Guo and Wang (1981) investigated the movement of summer rainbelt in China and its connection to EASM. The date of EASM onset varies geographically with respect to the propagation of EASM. Tao and Chen (1987) presented the first onset distribution map of EASM with results from their study and published literature. Zhu and Yang (1989) indicated that the summer rainbelt over East China had three distinct jumps during its northward movement based on 10 years raingauge observations. The three jumps marked the beginning of three unique features of summer rainfall activities over east China. They were defined as (1) the pre-raining season over south China, (2) Mei-Yu[1] over Yangtze River basin (YZRB) and (3) the rainy season over North China. Ding (2007) gives a detailed review on the Asian summer monsoon and its associated variability, in which the traditional view of two major jumps of the rainbelt and the associated shift of atmospheric circulations is well presented. They are corresponding to the Mai-Yu and rainy season in North China, respectively.

Many indices have been proposed in investigations of the Asia summer monsoon system (e.g., Chen et al. 1996; Lin and Lin 1997; Lau and Yang 1997; Wang and Wu 1997; Hsu et al. 1999; Wang and Fan 1999; Qian and Yang 2000; Ding and Liu 2001; Ding et al. 2004; Wang et al. 2004). Most of these indices are about onset of the South China Sea Summer Monsoon (SCSSM). Only two types of indices are related to descriptions of the EASM propagations. The first one is the precipitation index. Lau and Yang (1997) used the multiyear-pentad-mean isohyet of 6 mm day^{-1} to represent the northward progression process of the Southeast Asian summer monsoon, while Lin (1987) investigated the movement of summer rainbelt over East China using a ratio of the decadal rainfall to annual rainfall. Chen et al. (2001) analyzed the EASM onset processes with a new definition based on combination of ratios of 5-day, 10-day, and 15-day averaged rainfall to annual daily mean rainfall. However, the criteria of defining the onset of a rainy season vary by location due to the geographically heterogeneous characteristics of rainfall climatology. Wang and LinHo (2002) applied a single rainfall parameter to show the spatial-temporal characteristics of Asian-Pacific monsoon rainy system, in terms of domain, onset, peak, and withdraw processes.

The second one is the temperature/humidity index. For example, Tang and Huang (1983) determined the EASM northward propagation according to the contour of $\theta_{se} = 348$ K at 1000 hPa, while Webster et al. (1998) defined onset of the South Asian monsoon using the mean position of the 220 W m^{-2} contour of outgoing longwave radiation (OLR). Fasullo and Webster (2003) recently applied the flux of vertically integrated moisture to determine onset and withdrawal dates of the Indian monsoon. These results demonstrated that the processes of monsoon progression were different depending on what parameters were selected in the studies. In addition, some results were only based single annual dataset. Therefore, it would be worthwhile to investigate the climatological characteristics of EASM progressing processes over East China by considering both thermodynamic and dynamic factors in order to minimize the uncertainties in defining the EASM onset and its propagations using different parameters.

The interdecadal variability of the North Pacific atmosphere-ocean system has been well documented and a prominent climate shift of the system in mid-1970s is evident (e.g., Trenberth 1990; Chen et al. 1992; Trenberth and Hurrel 1994). The interdecadal variations of this system and their connections to precipitation and Asia monsoon have been observed and studied by many investigators. For example, Chang et al. (2000a, b) indicated a relationship between tropical Pacific sea surface temperature (SST) and EASM such as a wet EASM preceded by a warm equatorial eastern Pacific the previous winter, and followed by a cold equatorial eastern Pacific the following fall. However, this relationship was affected by the interdecadal variability of the coupled ocean – atmosphere system. Precipitation over the US Pacific coast shows the signal of interdecadal variation (Chen et al. 1996). The interdecadal variability is also seen in the

[1] Mei-Yu is traditionally defined as the rainy season from early June to early July over the Yangtze River and Huaihe River basins.

Indian monsoon-El Nino South Oscillation (ENSO) relationship and tropical storm activities in the western North Pacific Ocean (Kumar and Dash 2001; Krishnamurthy and Goswami 2000; Yumoto and Matsuura 2001). Many observational investigations revealed conspicuous summer climate changes in East Asia in the last several decades (e.g., Chen et al. 1998, 2004; Li et al. 2002). Previous results already show that the EASM variations are closely related to the climate changes (e.g., Ding 1992, 1994; Chang et al. 2000a, b). However, we currently still have inadequate knowledge on systematical understanding of EASM in terms of its advance and retreat processes at interdecadal timescales. Under different interdecadal background states, what are the changes of EASM in terms of onset, intensity, stage of northward propagation, and position of northern edge? How do those changes affect the summer droughts and floods in China? Study of these questions would further improve our understanding of the possible influences of the EASM interdecadal variability on the intraseasonal variations of EASM. Results could improve short-range climatic predictions on summer floods and droughts in China.

2. Methodology and datasets

2.1 Methodology

The magnitudes of summer rainfall in China do not fully represent the movement of summer rainbelt due to the large regional differences of precipitation climate. Tao et al. (1958) analyzed the movement of rainbelt in Mei-Yu period in term of the ratio of every 15-day rainfall in summer (May–August) to its total summer rainfall. Chen et al. (2001) defined a ratio of the N-day running mean daily rainfall to the annual mean daily rainfall as the relative precipitation coefficient (C_N) and applied it to study the advance/retreat processes of the summer rainy season in China. However, it is impossible to determine the movement of the summer rainbelt based on a unified criterion of C_N because of large regional differences of the annual mean daily rainfall. Therefore, in order to overcome the large regional differences in summer rainfall, a new precipitation index named as normalized precipitation index (NPI), is introduced so this variable can be regarded as a unified parameter across China:

$$\mathrm{NPI}(t) = \frac{R_5(t) - R_S}{\sigma_S} \quad (t = 1, 2, \ldots, n) \tag{1}$$

where $R_5(t) = \frac{1}{5}\sum_{i=-2}^{i=2} R(t+i)$ is a 5-day running mean daily rainfall for the ith day at any observation station, and R_S the summer (May–August) mean daily rainfall at this station, $\sigma_S = \left(\sum_{t=1}^{n}(R_5(t) - R_S)^2/n\right)^{1/2}$ the standard deviation of the 5-day running mean daily rainfall, and n is the total days of the summer. Thus, NPI(t) is actually the anomaly of the 5-day running mean daily rainfall from the summer mean daily rainfall normalized by its standard deviation.

The areas with relatively high NPI values are the locations of high summer precipitation. With this definition, NPI becomes a unified variable that is consistent for any region of China, regardless of whether there is more or less summer rainfall in this area. Therefore, the locations of the summer rainbelt over China could be consistently determined according to the movement of high NPI locations.

The equivalent potential temperature (θ_{se}) for a water-saturation pseudo-adiabatic process is calculated using the formula given by Bolton (1980):

$$\theta_{se} = T_k \left(\frac{1000}{p}\right)^{0.2854(1-0.28\cdot 10^{-3} r)} \cdot \exp\left[\frac{3.376}{T_L} - 0.00254 \cdot r(1 + 0.00081 \cdot r)\right] \tag{2}$$

where T_k, p, r are the absolute temperature, pressure, and mixing ratio at surface respectively, and T_L absolute temperature at the lifting condensation level.

The wavelet transfer technique (Morlet 1983) was applied to study the features of EASM variability in frequency domain. The advantage of the wavelet transfer technique is that it provides instantaneous estimates of amplitude and phase for each harmonics.

2.2 Datasets

The temperature, humidity and pressure fields from NCEP/NCAR reanalysis datasets for

1951–2001 (Kalnay et al. 1996) and ECMWF reanalysis datasets for 1958–2001 (Dethof et al. 2005) at 2.5° × 2.5° grid resolution were applied in this study. In addition, the CRU GMSLP2 datasets from 1958 to 1998 are also utilized in the analysis (Basnett and Parker 1997). We are aware that several studies question the reliability issues of the NCEP reanalysis datasets. Trenberth and Guillemot (1998) pointed out the large and significant biases in the NCEP moisture fields in the tropics. Newman et al. (2000) also showed serious discrepancies in the mean spatial structures over western tropic Pacific from NCEP precipitation field compared with European Center for Medium-Range Weather Forecasts (ECMWF) and the National Aeronautics and Space Administration (NASA) products. Kinter et al. (2004) demonstrated that the NCEP precipitation and divergence fields have obvious interdecadal shifts in the tropics. Recent studies by Wu et al. (2005) provide more evidence of the discrepancy of inderdecadal changes over Asian regions from the NCEP reanalysis datasets. These results suggest that caution should be used in applying the NCEP reanalysis outputs to study the interdecadal variability. Therefore, ECMWF and CRU datasets are used as an independent data sources to check results from the NCEP datasets.

The long-term surface daily rainfall observations from a dense raingauge network in China have been utilized for this study. The quality of the precipitation dataset from the rain gauge network is well documented (Zhai et al. 1999; Gong and Wang 2000; Gemmer et al. 2004; Wang and Zhou 2005). There were 686 standard surface rain gauge stations in China from 1 January 1951 to 31 December 2001; most of them are located in East China. However, the data record length varies among these stations. In addition, data interruptions exist at some stations. In order to have a best complete summer daily rainfall dataset (May 1–August 31) for this study, we selected 366 stations which had consistently uninterrupted summer daily rainfall observations in East China (>105° E) for 1957–2001. However, the summer monthly rainfall based on the datasets are reliable for 1951–2001. These selected stations in east China are shown in Fig. 1 which presents a well balanced and high resolution raingauge distribution. The rainfall dataset was spatially interpolated into 1° × 1° resolution using the scheme from Cressman (1959) in order to conduct consistent analyses at same spatial and temporal resolutions.

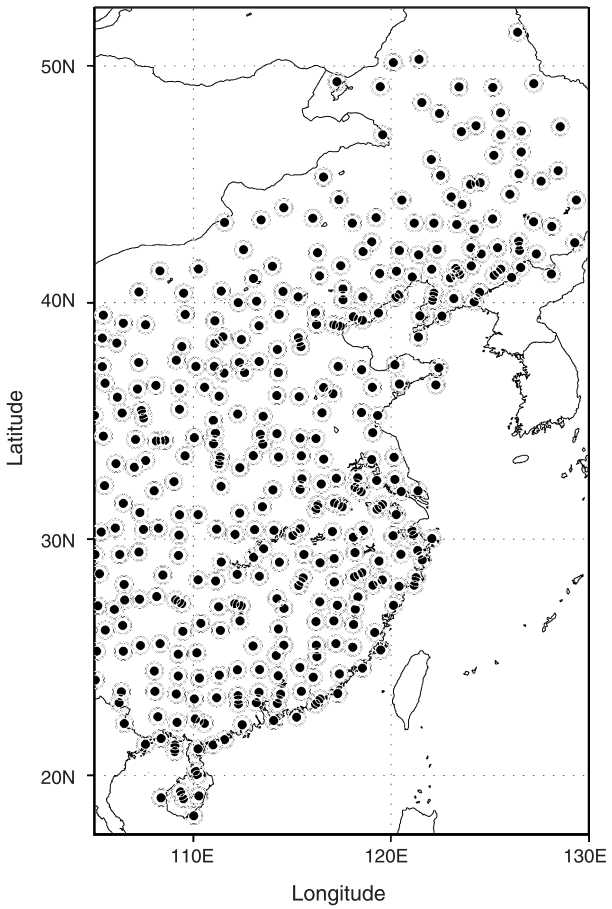

Fig. 1. The distribution of 366 selected surface raingauge stations in East China

3. Climatological characteristics of EASM northward propagation

3.1 Climatology of summer rain belt from NPI

The variations of climatological summer rainfall and NPI in East China are presented by the time-latitude section of a 5-day running mean daily rainfall and NPI averaged over 110–120°E for 1957–2000 from the raingage network measurements (Fig. 2). The northward advance of the maximum rainfall from South China in early May to North China in late July and early August is shown. The rainbelt withdraws quickly in mid-August. It is evident that the rainbelt has three prominent northward jumps during

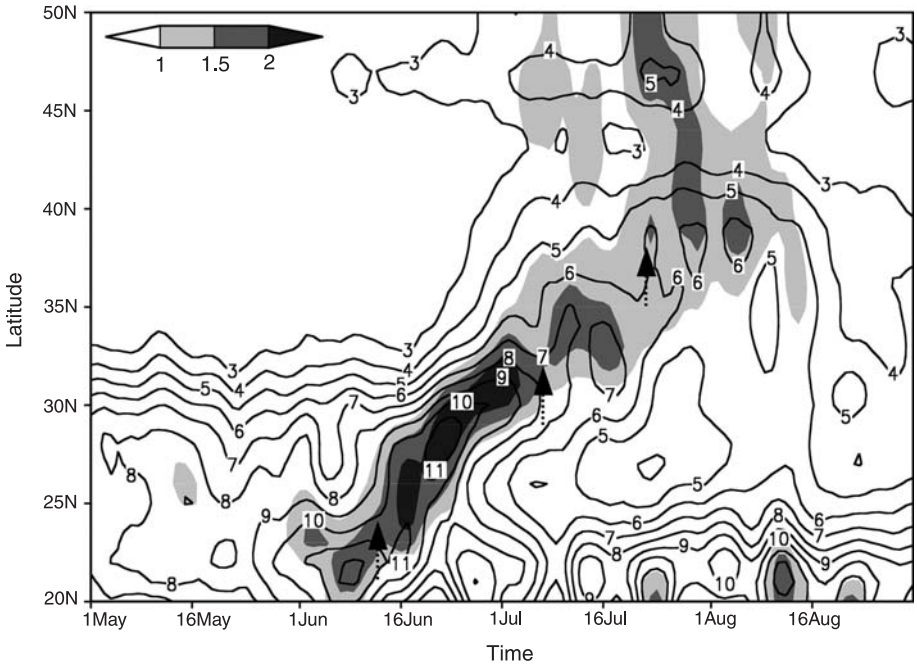

Fig. 2. Evolutions of the climatological 5-day running mean rainfall (solid lines, mm day^{-1}) and the unified precipitation index (shaded area) from May 1 to August 31 for 1957–2000 based on surface raingage observations averaged over 110–120° E. The heavy arrows ↟: denote the starting points of the three northward jumps of summer rainbelt in East China

the process. The first jump is in the 3rd pentad of June, and the second and third jumps are in the 2nd and 5th pentad of July, respectively. The northward propagations of the rain belt defined only by the variations of the maximum rainfall locations are quite complicated due to the inhomogeneous distributions of precipitation, large regional differences in rainfall magnitudes, and multiple relative maximum rainfall centers. However, area with NPI ($\geq$1) shows a relatively smooth movement, which corresponds very well to the rainbelt propagation. In addition, distributions of NPI ($\geq$1.5) reflect the maximum rainfall centers and its northward jumps. We define a NPI northward jump if the NPI ($\geq$1.5) position shifts more than 3 degree northward in 5 days, i.e., the northward propagation speed for a jump is about 150% faster than its mean speed of the northward movement. The NPI clearly shows three jumps marked by the heavy arrows during its northward propagations. The first jump in the 3rd pentad of June marks the onset of Yangtze River Mei-Yu, while the second jump in the 2nd pentad of July indicates the start of raining season in Huaihe River Mei-Yu. The third jump in the 5th pentad of July starts the rainy season of north China. The relative maximum magnitudes of NPI represent the strength of the positive anomaly of daily rainfall to its summer mean value. It is obvious that the most outstanding phenomenon of summer rainy systems in China is the Yangtze River Mei-Yu. The characteristics of the rainbelt northward propagation are consistent with the traditional view of the summer rain activities in China summarized by Ding (2007), except the Huaihe River Mai-Yu is identified from the NPI analysis. This Huaihe River Mei-Yu is categorized as part of the traditional Mei-Yu by previous studies, because it is hard to separate from the traditional Mei-Yu with the traditional rainfall analysis.

Similar features are shown in the horizontal distributions of pentad averaged rainfall and NPI (figure omitted). The propagations of NPI ($\geq$1.5) areas clearly better represent the movement of summer rainbelt in East China than the rainfall distribution, because NPI is a unified parameter that could eliminate uncertainties due to inhomogeneous rainfall distributions.

In summary, the newly defined parameter NPI ($\geq$1.5) is a better indicator of describing the northward movement of summer rain systems in East China. It shows three jumps of the summer rainbelt, which mark the beginnings of three rainy seasons in East China, i.e., Yangtze River Mei-Yu, Huaihe River Mei-Yu, and rainy season in north China. Also, the magnitude of NPI represents systematically strength of the rain systems.

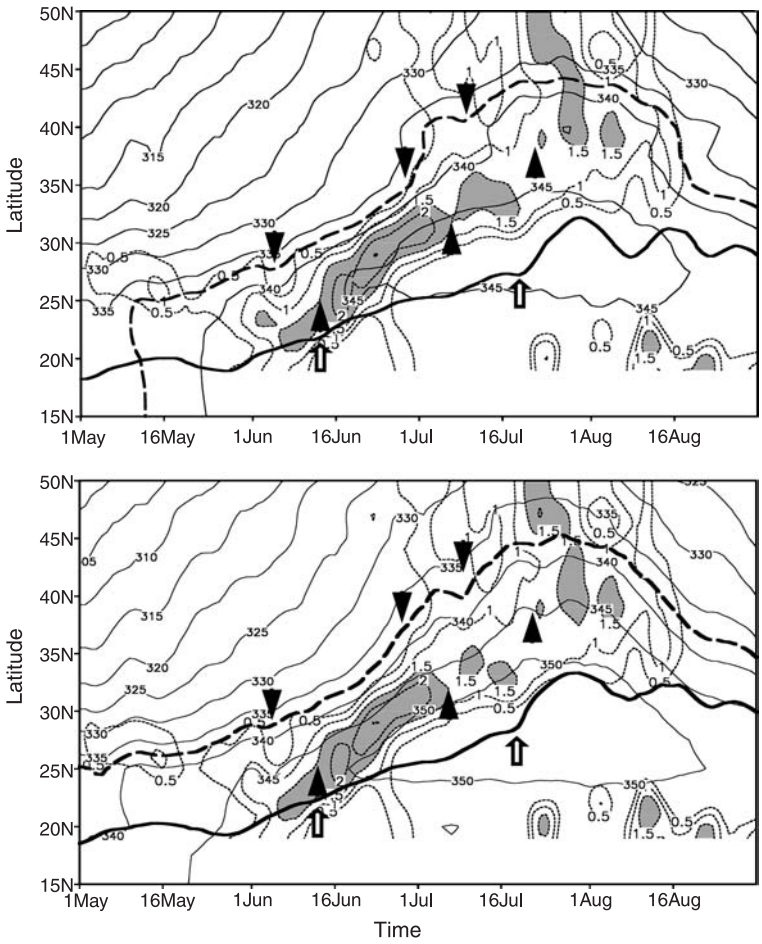

Fig. 3. Evolutions of the climate 5-day running mean θ_{se} at 850 hPa (solid lines, the contour $\theta_{se} = 337.5$ K is shown as heavy dashed line) and the unified precipitation index (dashed lines, areas with NPI ≥ 1.5 are shaded) averaged over 110°–120° E, the latitudes of $U = 0$ at 500 hPa (heavy solid line) averaged over 125°–145° E from May to August for NCEP 1957–2000 dataset (top panel) and for ECMWF 1958–2000 dataset (bottom panel). NPI is based on the surface rain gauge network observations over east China. The positions of the West Pacific subtropical high ridge, EASM leading edge, and summer rainbelt in East China are shown by the contours of $U = 0$ at 500 hPa, $\theta_{se} = 337.5$ K at 850 hPa and NPI = 1.5, respectively. Their northward jump points are marked by ⇧, ▼, and ▲, respectively

3.2 EASM propagation and variation of West Pacific subtropical high

Study by Tang and Huang (1983) suggest that the summer saturated equivalent potential temperature (θ_{se}) at 850 hPa over East China and its coastal areas is generally greater than 336–340 K. They indicat that the area with θ_{se} between 336 and 340 K at 850 hPa could be taken as the EASM northern edge. The seasonal variations of the West Pacific subtropical high (WPSH) also play an important role in the advance/retreat of EASM. For example, recent study by Wu et al. (2002) show that the boundary of easterly and westerly wind (i.e., $U = 0$) of the subtropical high at 500 hPa could fairly reflect the continuous variations of the subtropical high ridge. However, relationship between the summer rainbelt movements, the EASM northward propagation, and the ridge position of WPSH has not been well investigated.

Figure 3 exhibits evolution of the climatically averaged 5-day running mean θ_{se} at 850 hPa over 110–120° E and $U = 0$ at 500 hPa over 125–145° E from May to August for 1957–2000 NCEP dataset (top panel) and 1958–2000 ECMWF dataset (bottom panel). The WPSH domain (125–145° E) is based on the definition by Wu et al. (2002). For comparison, contours of the associated NPI are also overlapped with shaded areas of NPI ≥ 1.5. We define a jump occurred when the WPSH ridge moves northward more than 1.5 latitudes in 5 days (which is about 150% of its mean propagation speed). Similarly, a jump of the EASM northern edge starts when the contour $\theta_{se} = 337.5$ K moves more than 2 latitudes in 5 days (which is about 200% faster than its mean speed).

The top panel shows that θ_{se} over the South China Sea rapidly exceeds 337.5 K, and jumps from 10° N into 25° N in the third pentad of May, which marks the onset of SCSSM. The ridge of WPSH withdraws southward and then follows a jump northward in late May. Since this jump occurs before the major raining system in

Table 1. Characteristics of monsoon indices during the EASM northward propagation. The date indicates a pentad in which a jump occurred while the latitude change shows a distance that the index position propagated northward in 5 days. The P# denotes for the # pentad of a month. * Indicates that a jump was not significant

Indices	First jump		Second jump		Third jump	
	Date (pentad)	Latitude change	Date (pentad)	Latitude change	Date (pentad)	Latitude change
$\theta_{se} = 331.5$ K (850 hPa)	P2 Jun.	27.5–29.5° N	P6 Jun.	34.5–37° N	P2 July	40.5–43° N
$U = 0$ (500 hPa)	P3 Jun.	22–24° N	P2 July*	25–26.5° N	P4 July	27–30° N
NPI = 1.5	P3 Jun.	25–28° N	P2 July	32.5– 36° N	P5 July	36–50° N

East China, we did not designate it in Fig. 3. Three obvious jumps of EASM are evident from late May to early August during the northward propagation processes. The $\theta_{se} = 337.5$ K makes the first jump from 27.5° N into 29.5° N in the second pentad of June, and the ridge jumps northward from 22 to 24° N in the third pentad of June, while the NPI = 1.5 jumps from 25 to 28° N which indicates the start of the Yangtze River Mei-Yu in the third pentad of June. The second jump of $\theta_{se} = 337.5$ K from 34.5° N into 37° N is in the sixth pentad of June, while the areas with NPI $\geq$ 1.5 moves to the Huaihe River basin in the second pentad of July. Although the ridge propagates northward from 25° N into 26.5° N in the second pentad of July, it does not fit the definition of a jump. However, it is still evident there is quick northward movement. The contour $\theta_{se} = 337.5$ K jumps the third time from 40.5° N into 43° N in the second pentad of July, the ridge propagates rapidly northward from 27° N into 30° N in the fourth pentad of July, which indicates the end of Huaihe River Mei-Yu. The rainy season in northern China starts in the fifth pentad of July. Similar features are evident from the ECMWF data analysis (bottom panel), although the magnitudes of the 1st and 2nd jumps of $\theta_{se} = 337.5$ K appear a little weaker than that from NCEP data. The detailed numbers associated with these jumps are listed in Table 1.

In summary, variations of contour $\theta_{se} = 337.5$ K at 850 hPa represent well the northward progressing process of the EASM leading edge. The northward advance and jump of $\theta_{se} = 337.5$ K at 850 hPa and the ridge of WPSH at 500 hPa are in very good agreement with the northward movements and jumps of rainbelt in East China. It is also worth pointing out the consistencies of first two jumps among for $\theta_{se} = 337.5$ K, $U = 0$ and NPI = 1.5 over Yangtze River and Huaihe-River basins, although the $\theta_{se} = 337.5$ K and WPSH ridge ($U = 0$) jumps are relatively weak with the Huaihe River rainy season. This demonstrates that there are two separate stages of Mei-Yu over the Yangtze River and the Huaihe-River basins. These findings support our classifications of dividing the traditional Mei-Yu into Yangtze River Mei-Yu and Huaihe-River Mei-Yu. However, the classification of Huaihe Mei-Yu is somewhat contradict to the traditional view of Mei-Yu reviewed in Ding (2007). Actually, our results are not opposite to the common view of Mei-Yu, except we are here trying to point out the different characteristics of rainy season over the Huaihe River basin from the Yangtze River region. Obviously, further investigations are needed to understand the thermodynamic and dynamical characteristics of the Mei-Yu systems.

4. Interdecadal variation of EASM northward propagation

In middle-late 1970s, the air–sea systems over the North Pacific underwent a remarkable interdecadal change, and observational evidence indicated that the East Asian summer climate also changed conspicuously (e.g., Chen et al. 1998; Li et al. 2002). The question arises as to whether there is an interdecadal change in the EASM northward propagation. Shown in Fig. 4 are time-latitude cross sections of May–August 5-day running mean NPI and $\theta_{se} = 337.5$ K averaged over 110–120° E at 850 hPa, and latitude of $U = 0$ over 125–145° E at 500 hPa for two distinct interdecadal climate systems in 1957–1978 and 1979–2000 from NCEP data (Fig. 4a and b), and in 1958–1978 and 1979–2000 from ECMWF data (Fig. 4c and d).

The NCEP dataset (Fig. 4a and b) demonstrates that the prominent characteristics are

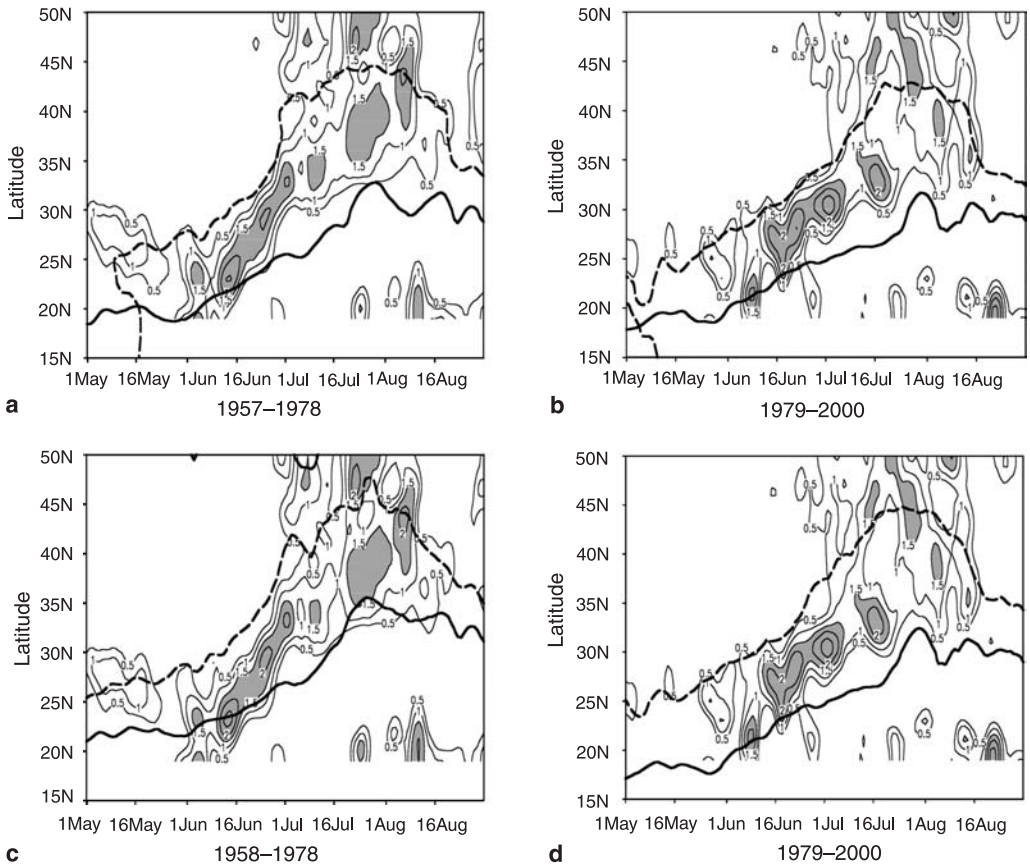

Fig. 4. Time-latitude cross sections of the climatological 5-day running mean unified precipitation index (solid lines, areas with NPI ≥ 1.5 are shaded) averaged over 110–120° E in East China from May to August for two distinct climate environments from surface rain gauge network observations: (**a**) 1957–1978 and (**b**) 1979–2000. The contour $\theta_{se} = 337.5$ K at 850 hPa (heavy dashed line) averaged over 110–120° E, and the latitudes of $U = 0$ at 500 hPa (heavy solid line) averaged over 125–145° E from NCEP dataset for these two time periods are overlapped. Similar plots of $\theta_{se} = 337.5$ K at 850 hPa and $U = 0$ at 500 hPa from ECMWF and NPI are shown in (**c**) 1958–1978, and (**d**) 1979–2000

different from 1957–1978 to 1979–2000. The ECMWF data (Fig. 4c and d) also shows different features from 1958–1978 to 1979–2000. It is evident that both NCEP and ECMWF datasets present similar results. The EASM northward propagation of NPI showing the summer rainbelt activities in East China is consistent with both contour $\theta_{se} = 337.5$ K and $U = 0$. Sensitivity tests with different selections of the breaking time in 1970s lead to similar conclusions. Results suggest that at interdecadal timescales there are two different kinds of EASM northward propagations in the past 40 years. The basic characteristics of the first one (for time before middle 1970s) include a fast northward propagation, a north border reached beyond its climatological position, and a longer duration over northern China. Thus, there was more rainfall in North China and less rainfall during Mei-Yu over the Yangtze River valley. The main characteristics of the second kind of EASM system include a slow northward movement, a northern border located relatively in the south of its climatological position, and a shorter duration over northern China. This leads to more Mei-Yu rainfall and less rainfall over northern China.

For further investigation of EASM differences between 1957–1978 and 1979–2000, Fig. 5 shows the time-latitude cross sections of May–August NPI anomalies over 110–120° E. It can be seen that the prominent negative NPI anomaly during 1957–1978 appears at 26–34° N from the 1st pentad of June to the end of August, indicating less Mei-Yu rainfall. The first positive NPI anomaly center is located in 20–26° N before the 4th pentad of June, which indicates more rainfall over southern China. Another positive center is located beyond 34° N from late June to August, which corresponds to more rainfall in North China. The almost opposite features

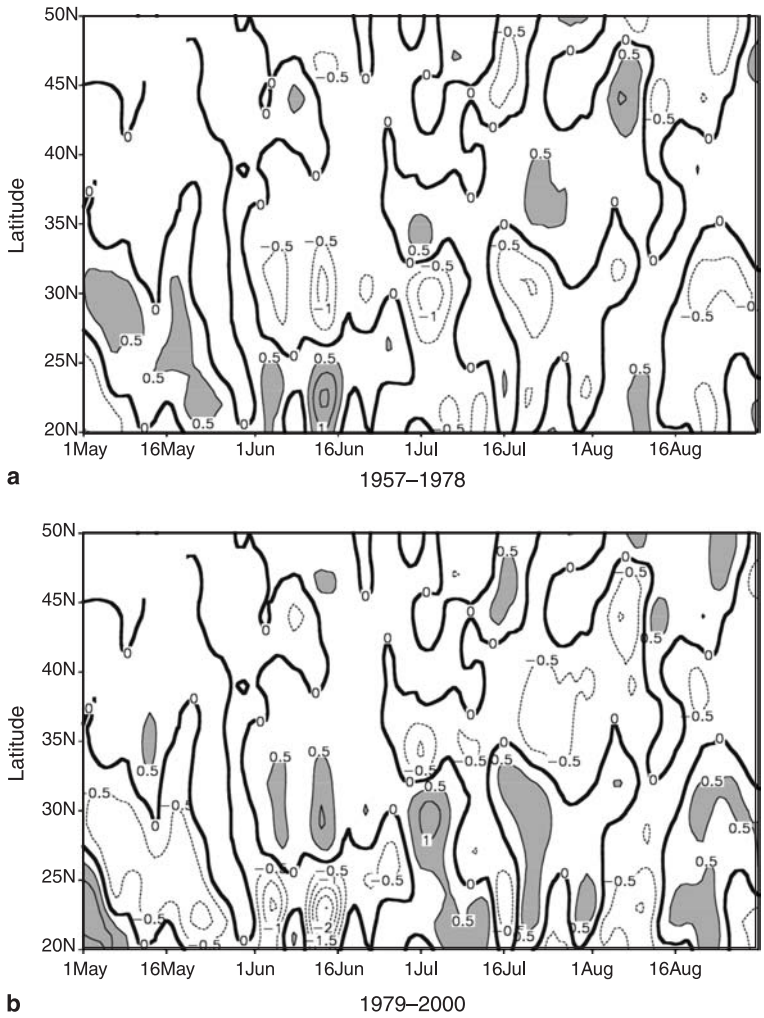

Fig. 5. Time-latitude cross sections of the NPI anomalies averaged over 110–120° E in East China from May 1 to August 31 for (**a**) 1957–1978 and (**b**) 1979–2000. Areas with values equal to or greater than 0.5 are shaded. Dashed lines are for negative values. The NPI = 0 contour is highlighted

are expected for 1979–2000 (Fig. 5b). These results are consistent with the previous findings by Li et al. (2002). Results here demonstrate that the EASM and associated summer rainbelt in East China have a clear interdecadal variation.

5. Influence of interdecadal variation of the EASM northern edge on summer precipitation in East China

Discussion from previous sections has shown that the interdecadal variation of the EASM northward propagation is evident, and there is a close relationship between the EASM progressing and the movement of summer rainbelt in East China. The northern edge of EASM is considered as one of the most important indices of the EASM activities based on the following two aspects. The first is the EASM coverage, which has very important influences on summer rainfall in China, especially in north China. The second is that Lian et al. (2003) demonstrated that the onset of summer monsoon in North China is closely related to the EASM strength. There will be an early onset of summer monsoon in North China with strong EASM, and vice versa. However, what is the spatial-temporal relationship between the northern edge and the strength of EASM? Since the north edge of EASM could be represented by its position and/or strength, what is the relationship between its position and strength? What is the impact of this relationship on summer floods and droughts in China? It is obvious that any answers to these questions would be helpful in improving climate predictions of wetness/dryness in East China.

5.1 Variations of EASM northernmost position and intensity

It has been demonstrated in Sect. 4 that the position of $\theta_{se} = 337.5$ K at 850 hPa can depict very

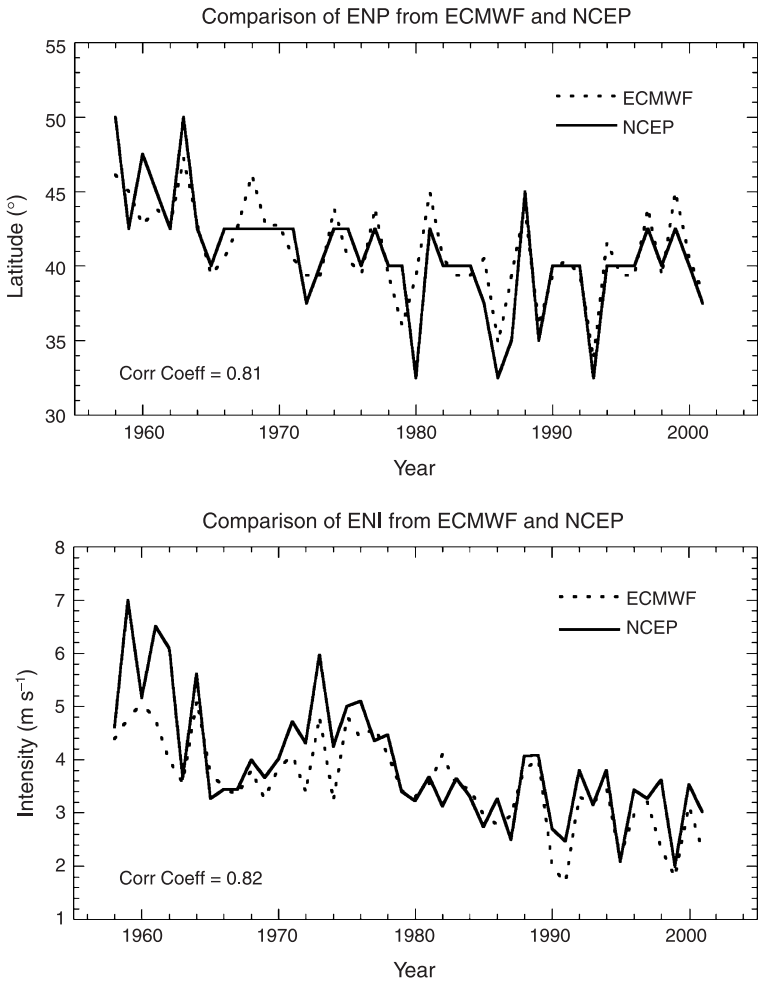

Fig. 6. Comparison of ENP (top panel) and ENI (bottom panel) between ECMWF and NCEP. Their correlation coefficient is shown at the bottom left corner

well the northward propagation of the EASM northern edge in East China. The EASM northernmost position (ENP) is then defined as the northernmost latitude of 5-day running mean θ_{se} which is ''consistently'' equal to or greater than 337.5 K at 850 hPa over 110–120° E. The ''consistently'' means that the 5-day running mean $\theta_{se} \geq 337.5$ K persists for at least 10 days of any 3 continuous pentads. Similarly, the EASM northernmost intensity (ENI) is defined as the mean southerly wind ($V>0$) at 850 hPa over the southern area of 2.5-latitude inside 110–120° E of ENP. The selection of 2.5° latitude is for the spatial resolution of NCEP reanalysis dataset.

The comparison of ENP and ENI from NCEP and ECMWF datasets is shown in Fig. 6. It is evident that the temporal variations of ENP from NCEP are consistent with that from ECMWF. Similar time series are obvious for ENI between NCEP and ECMWF, except NCEP shows a relatively strong intensity. The related correlation coefficient for ENP and ENI between NCEP and ECMWF is 0.81 and 0.82, respectively. Results demonstrate the classifications and temporal variations of ENP and ENI are reliable. Figure 7 presents the ENP time series for 1951–2001 and its wavelet analysis based on the NCEP/NCAR reanalysis daily dataset. Both interannual and interdecadal variations are evident, however, the prominent interdecadal change occurred around 1964. A running *t*-test of the time series (i.e., a method of change-point analysis) indicates that the interdecadal variation is significant at a 1% significance level. The averaged ENP is at 47° N for 1951–1964, while only at 39° N for 1965–2001. The overall mean position is at 42° N. The Morlet wavelet analysis could transfer the ENP characteristics at time domain into frequency domain so that the dominant mode of variation would be easily identified (Torrence and Compo 1998; Jiang et al. 2003). The thick

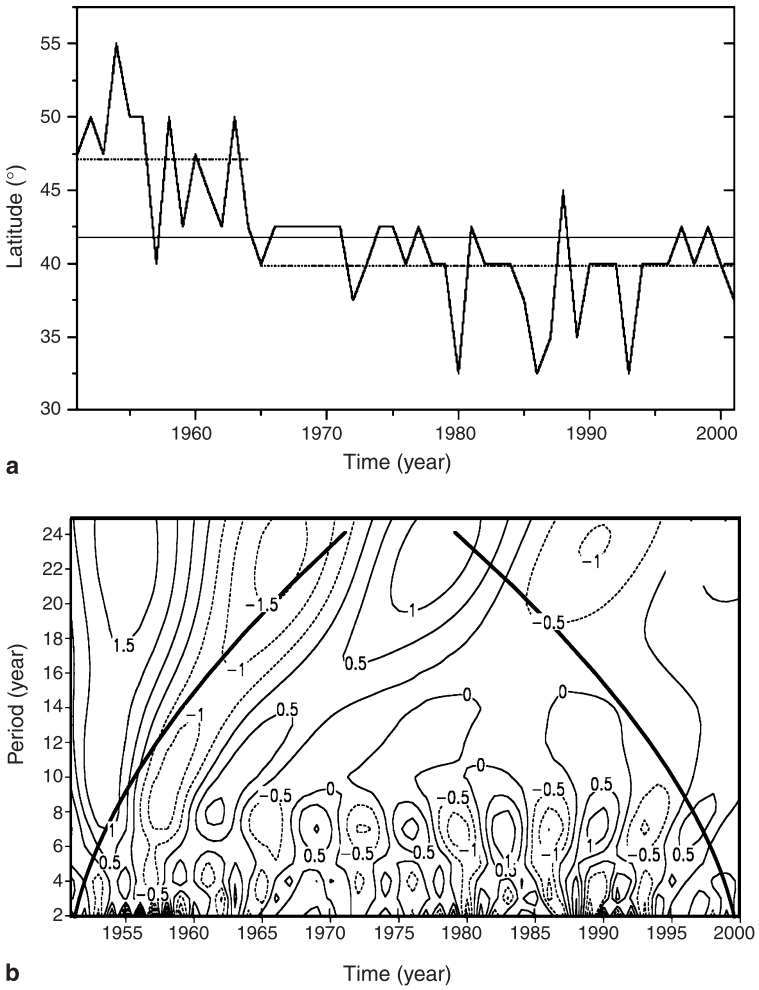

Fig. 7. Top panel is the temporal evolution of the EASM northernmost position (ENP) averaged over 110–120° E in East China during 1951–2001. The light horizontal line is climate mean position while the dash lines are the mean positions before and after climate change in middle of 1960s. Bottom panel is the distribution of the real part of Morlet wavelet transformation coefficient of the ENP averaged over 110–120° E during 1951–2001. The overlapped heavy lines denote the ''cone of influence''

solid lines in Fig. 7b denote the ''cone of influence'', which means that the edge efforts become important over regions outside the cone. It is obvious that ENP has two dominant frequencies at time periods of 6–8 years and 20–22 years. Due to the limited length of the time series, the 20–22 year frequency is influenced by the fringe impact of the time series. Similar analyses are conducted for ENI (Fig. 8). An obvious change was around 1964, however, the prominent change point of the interdecadal variation is around 1978 (Fig. 8a). The averaged ENI is $4.5\,\mathrm{m\,s^{-1}}$ for 1951–1978, while only $3.2\,\mathrm{m\,s^{-1}}$ for 1979–2001. The overall mean intensity is $3.75\,\mathrm{m\,s^{-1}}$. The time period of its dominant frequency is 12–16 years from the Morlet wavelet analysis (Fig 8b). Therefore, the interdecadal variation is evident for both ENP and ENI. However, the differences between ENP and ENI exist at the period of their interdecadal variability and ENP shifted earlier than ENI. These might be due to the fact that ENP and ENI are two different parameters of EASM. They are not highly correlated, although they could be used to present the strength of EASM. This feature also indicates the complex nature of EASM.

Due to the obvious interannual and interdecadal variations of ENP and ENI, the correlation coefficients between ENP and ENI were calculated with raw data, low pass filtered for over 7 years and high pass filtered for less than 7 years (Table 2). The band filtering technique was adapted from Zheng and Dong (1986). The raw ENP and ENI have a positive correlation, while their interannual relationship is negative. In addition, there is a significant correlation coefficient of 0.53 at 5% significance level between ENP and ENI at interdecadal timescale. Results indicate that there are two different kinds of relationships between ENP and ENI, i.e., at interdecadal timescales, the more northern the position of ENP, the greater the intensity of ENI; at inter-

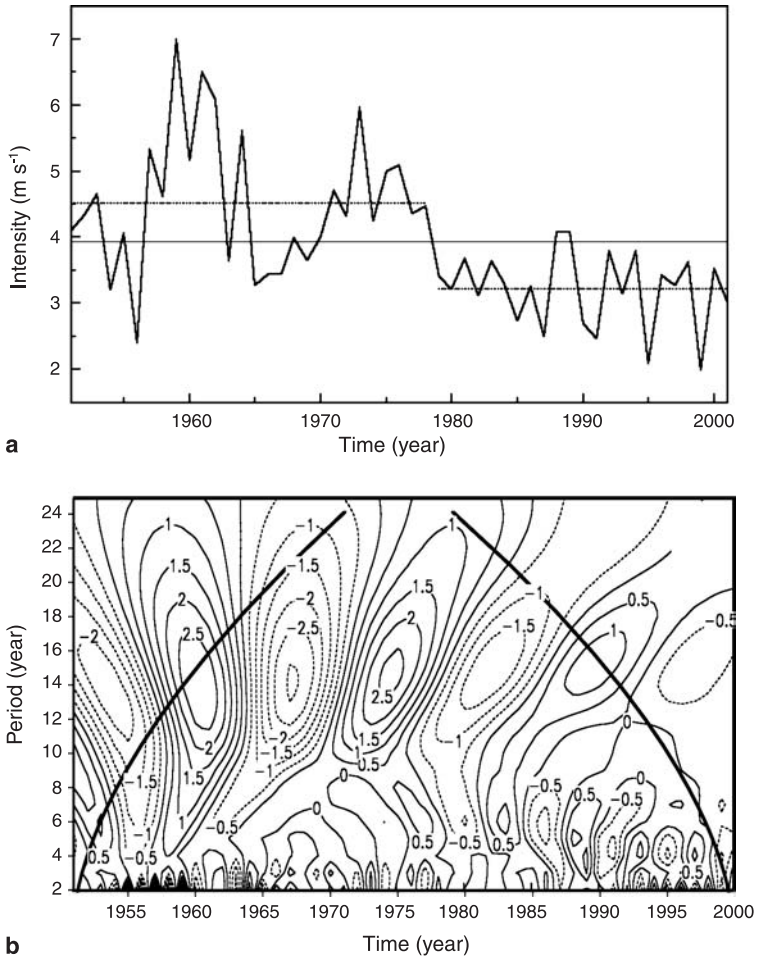

Fig. 8. Same as Fig. 7, except for EASM northernmost intensity (ENI)

Table 2. Correlation coefficients between summer monsoon index (SMI), the EASM northernmost position (ENP), and intensity (ENI) at raw data, interannual timescale (with a <7-year band filter), and interdecadal timescale (with a >7-year band filter)

	Raw data	Interannual variation	Interdecadal variation
SMI-ENP	−0.59	−0.24	−0.81
SMI-ENI	−0.61	−0.24	−0.82
ENP-ENI	0.21	−0.22	0.53

annual timescales, the more northern the position of ENP, the lesser the intersity of ENI. However, the relationship between ENP and ENI is most significant at interdecadal variation. Those results are consistent with what found in Figs. 7 and 8.

Shi et al. (1996) introduced a summer monsoon index (SMI), defined as the difference between the boreal summer averaged sea level pressure (SLP) from 20 to 50° N at 110° E and 160° E, to represent the strength of EASM. The summer continental SLP over China is generally lower than the west Pacific SLP at same latitudes so that the SMI is a negative value whose magnitude is proportional to the EASM intensity. Thus, the positive SMI indicates a relative weak EASM while negative SMI is for relative strong EASM. Figure 9 shows a comparison of time series of SMI, ENP, and ENI anomalies normalized by their standard deviations. It is evident that there is a generally consistent interdecadal variability among SMI, ENP, and ENI, although their interannual variations are not consistent. The correlation coefficients at different timescales are listed in Table 2. The significant negative correlations between SMI and ENP and between SMI and ENI at interdecadal timescale indicate that ENP is beyond its normal position and ENI is above normal when EASM is strong, and vice versa. For instance, EASM is relatively weak after late 1960s while ENP is at south side of its normal position. The ENI became smaller and shown a climate change while ENP moved southward from its normal position and EASM further

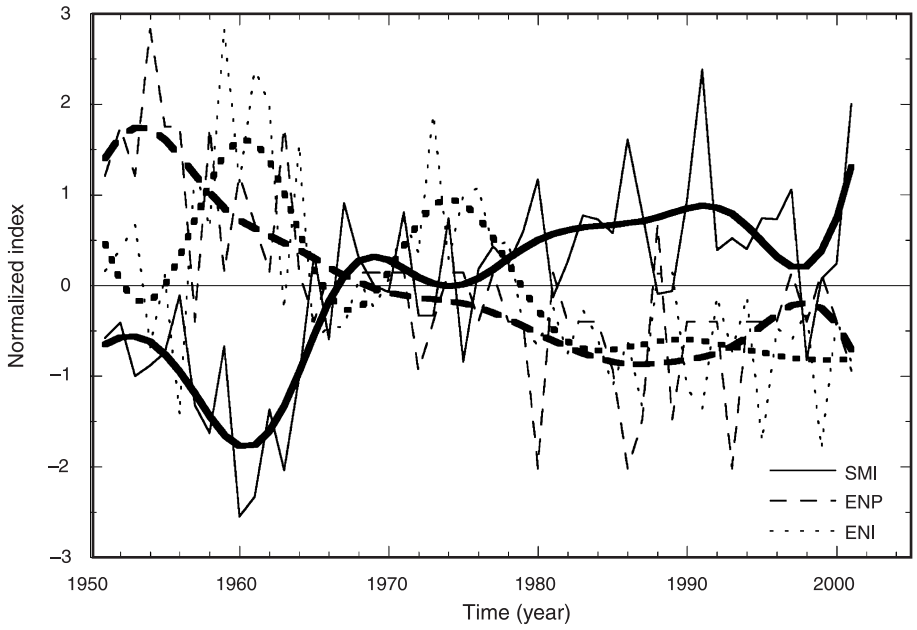

Fig. 9. Comparisons of the anomalies of Asia summer monsoon index (SMI), EASM northernmost position (ENP), and EASM northernmost intensity (ENI) normalized by their standard deviations from NCEP 1951–2001 datasets. The associated thick lines are the smoothed time series, respectively

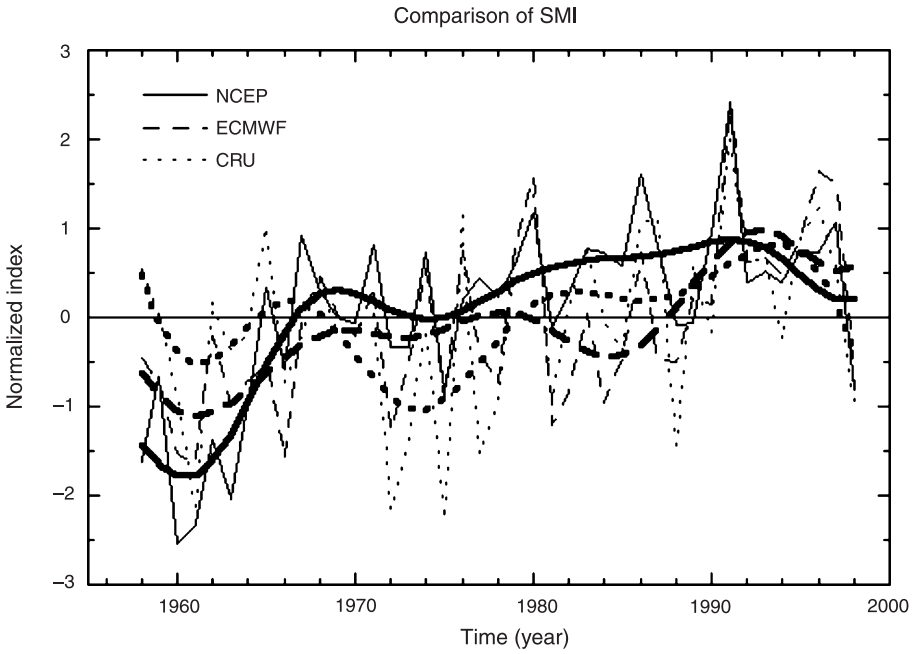

Fig. 10. Comparison of SMI time series from NCEP, ECMWF and CRU during 1958–1998. The associated thick lines are the smoothed time series, respectively

weakened since late 1970s. However, SMI and ENP (or ENI) do not have a significant relationship at interannual timescales. The differences of relationships among SMI, ENP, and ENI at interannual and interdecadal timescales suggest that different physical processes at different timescales might work together to generate this complicate feature of EASM.

Figure 10 shows comparison of normalized SMI for 1958–1998 from NCEP, ECMWF and CRU datasets. The ECMWF and CRU datasets are applied to check the NCEP SMI analysis. It is obvious that NCEP, ECMWF and CRU SMI exhibit a similar trend from strong to weak EASM and an interdecadal variation. The CRU SMI shows a major shift in late 1970s. The SMI correlation coefficient is 0.56 and 0.75 between NCEP/ECMWF and ECMWF/CRU, respectively. However, discrepancies are also evident, such as the NCEP data indicates above normal

SMI from late 1960s, especially from middle 1970s, while the ECMWF data shows SMI changed from below to near normal in late 1960s and above normal in late 1980s. The CRU SMI varies negatively before the late 1970s, and stays positive after that. Thus, the NCEP reanalysis presents a relatively stronger interdecadal variation than the ECMWF and CRU datasets. Results suggest that the characteristics of interdecadal variation from NCEP datasets alone should be evaluated with other independent datasets. Those are consistent with previously published literature (e.g., Wu et al. 2005; Kinter et al. 2004). Another test on NCEP SMI has been conducted to check a different SMI definition based on the land-sea thermal difference (Sun et al. 2004). With surface soil temperature and sea surface temperature from 1961 to 1999, the new SMI illustrates a strong (weak) Asian summer monsoon before (after) middle 1970s (figure not shown). This kind of temporal variation is consistent with that from the NCEP SMI. Therefore, the interdecadal change of SMI based on NCEP dataset is reliable, although uncertainties exist.

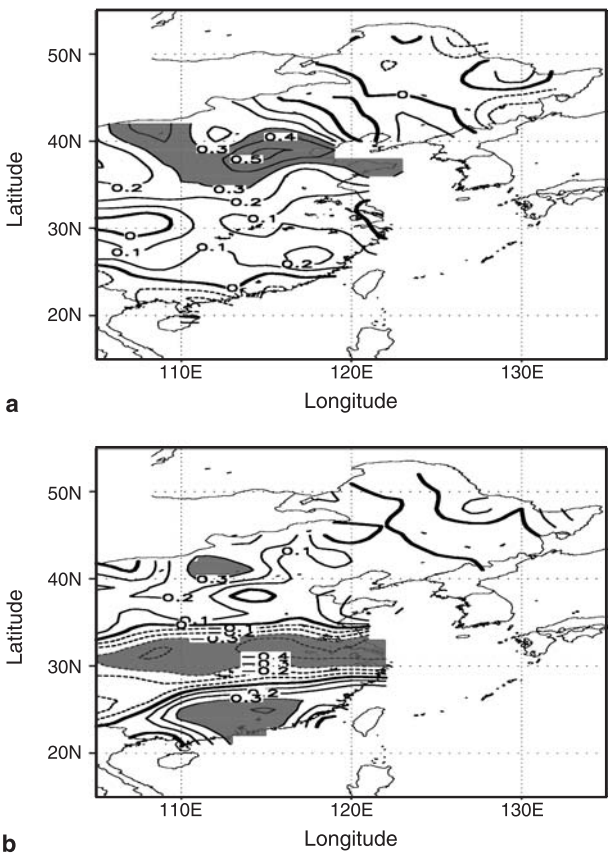

Fig. 11. Distributions of correlation coefficients between the summer rainfall (May–August) in East China for 1951–2000 with ENP (**a**) and ENI (**b**). The shaded regions are at 5% significance level. Dashed lines are for negative correlation coefficients

5.2 Influences of ENP and ENI variations on summer precipitation in East China

Figure 11a shows the distributions of correlation coefficients between the summer (May–August) rainfall in east China and ENP during 1951–2000. The correlation coefficients equal to or greater than 0.3 are at 5% significance level and are shaded. It is obvious that significant positive correlations exist over the North China-Inner Mongolia regions. Results indicate that there will be more rainfall when ENP is at the northern side of its normal situation, and vice versa. This is understandable because the farther north the EASM reaches, the more moisture is brought to North China. Therefore, more precipitation would be in North China.

Figure 11b presents the distribution of correlation coefficients between summer rainfall and ENI in East China. Significant negative correlations are evident over the Yangtze River basin, while there are significant positive correlations in South China and East of Inner Mongolia. These results suggest that the stronger the ENI, the more summer precipitation in both south China and east of Inner Mongolia and less summer rainfall in the Yangtze River basin; and vice versa. It also suggests that summer rainfall anomaly in south China and Yangtze River basin are in opposite directions. When there is a positive anomaly of summer rainfall in South China, there would be a negative anomaly of summer precipitation in the Yangtze River basin and a small positive anomaly of summer precipitation in the North China–Inner Mongolia region. This kind of summer precipitation distribution in East China is similar to the distribution of category-I summer rainfall pattern given by Liao and Zhao (1992).

For further investigation of these regional characteristics between EASM and summer rainfall in East China, summer rainfall is divided into three sub-regions which have well distributed basic stations. We selected these stations [North China (15), Yangtze River basin (22),

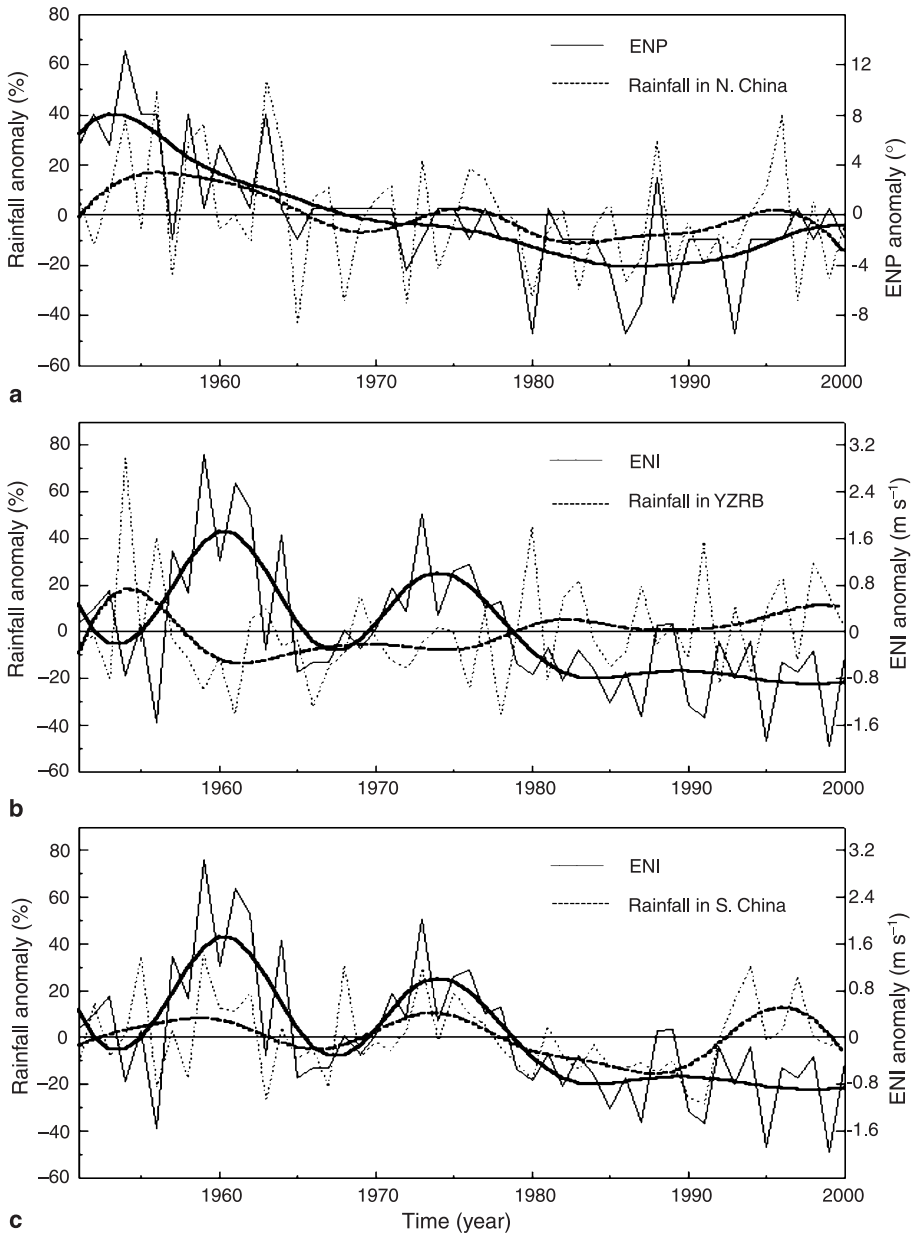

Fig. 12. Top panel shows time series of summer rainfall anomaly (dashed lines) over northern China and ENP (solid lines). Middle panel is for summer rainfall anomaly over Yangtze River basin (YZRB, dashed line) and ENI (solid line). Bottom panel is same as middle panel except for summer rainfall anomaly over southern China. Their $\geq$7 years band filtered time series are shown as heavy lines. The left y-axis is for summer rainfall anomaly, while the right y-axis is for ENP or ENI anomaly

and South China (14)] that have correlation coefficients better than 0.35 with ENP and/or ENI for Fig. 12, which are time series of anomalies of ENP, ENI, and mean summer rainfall over these regions for 1951–2000. Figure 12a shows percentage of time series of the summer rainfall anomaly in north China and the ENP anomaly. It is obvious that variations of these two time series are generally consistent. Good correlation is clearly seen in a $\geq$7 years band filtered time series. Both have positive anomalies before 1970s while negative anomalies after early 1970s. The anomalies of ENI and summer rainfall over Yangtze River basin are shown in Fig. 12b. The interdecadal variations of ENI and summer rainfall anomalies are evident and there is relatively good negative correlation between these two time series, such as a positive anomaly of ENI corresponding to a negative anomaly of summer rainfall from late 1950s to late 1970s; and vice versa after late 1970s, although there is an obvious drop of ENI in middle 1960s but that is not at the interdecadal scale. Similar analysis is conducted in South China (Fig. 12c). The silent feature is the similar patterns of ENI and summer rainfall anomalies, and their good relationship at interdecadal timescales. However, we have to point out the different interdecadal be-

Table 3. Correlation coefficients between EASM northernmost position (ENP), intensity (ENI), and summer rainfall over north China, Yangtze River basin and South China. Numbers in parentheses are for >7-year band filtered time series

	North China	Yangtze River basin	South China
ENP	0.52 (0.81)	0.08 (0.08)	0.07 (0.41)
ENI	0.15 (0.62)	−0.47 (−0.67)	0.54 (0.52)

havior of rainfall in North China and Yangtze River basin/South China, which is closely correlated to the ENP and ENI interdecadal variations, requiring further investigation.

Detailed correlation coefficients among these variables in North China, Yangtze River basin and South China are given in Table 3. Numbers inside parentheses are based on $\geq$7 years band filtered time series. It is evident that ENP and summer precipitation have no significant relationship over the Yangtze River basin and South China, while there is a significant correlation in North China. The ENI and summer rainfall have a positive, negative, and no relationship in South China, Yangtze River basin, and North China, respectively. The relationships are enhanced at interdecadal time scale. For example, the interdecadal variations of summer rainfall and ENP have a significant correlation in South China, while ENI and summer rainfall have a very close relationship in North China. These results demonstrate that the impacts of ENP and ENI on summer rainfall in East China are important, and the influences cover almost entire East China.

In summary, the large-scale summer precipitation anomaly in East China has a complex but good relationship with ENP and ENI at interdecadal scale. Rainfall in North China has a significant positive relationship with ENP, while Rainfall over the Yangtze River basin shows a strong negative relationship with ENI. In addition, a significant positive relationship exists between ENI and rainfall in South China. Different characteristics of ENP and ENI interdecadal variability are also evident. The major shift of ENP is around the middle 1960s, while in later 1970s for ENI. This feature indicates the position and intensity of EASM are not well correlated at interdecadal scale, exhibiting a complex nature of EASM northward propagations.

6. Discussion and conclusions

This paper describes interdecadal variations of the EASM northward propagation using NPI, EASM northern edge, and WPSH ridge as well as SMI based on daily rainfall measurements from 366 basic stations in China for 1957–2001, NCEP/NCAR reanalysis products for 1951–2001, ECMWF reanalysis dataset for 1958–2001, and CRU datasets for 1958–1998. The relatively stronger interdecadal variation of EASM from NCEP than from ECMWF/CRU is in agreement with the reported climate systematic bias in the tropics (e.g., Kinter et al. 2004; Wu et al. 2005). However, the generally consistent characteristics of interdecadal variations among these different independent datasets analyzed in this study demonstrate that NCEP/NCAR reanalysis could still be useful in examining interdecadal variability of the EASM northward propagations and its impact on the summer rainfall in East China with an acceptable degree of uncertainties.

NPI is defined as a 5-day running mean daily rainfall anomaly from the summer mean daily rainfall normalized by its standard deviation so that differences in defining the summer rainbelt movement due to regional rainfall variations could be eliminated. Since regional climate of summer rainfall varies substantially across China, it is unreasonable to compare the relative magnitudes of regional rainfall over such a large area. However, the newly defined NPI could unify precipitation at different regions so that NPI magnitude at any region could be compared to reveal locations of abnormal rainfall occurrences. ENP is defined as the summer northernmost position of $\theta_{se} = 337.5\,\mathrm{K}$ in East China. The averaged southerly wind speed within the area of 2.5° south side of the ENP is applied to define ENI. In addition, relationships between ENP, ENI, and the strength of EASM are investigated.

Analyses of NPI and its relationships with atmospheric thermodynamic and dynamic conditions as well as temporal evolutions, present a complex picture of the EASM northward propagations and interdecadal variations. Results suggest important influences of interdecadal variation of the EASM northward propagation on summer rainfall in East China. The contour NPI = 1.5 could accurately represent activities

of the summer rainbelt in East China in terms of southward/northward movement, abruptly northward jumps, and durations of rainbelts. After onset of the summer monsoon over South China Sea in late May, the climatological summer rainbelt generally undergoes three northward jumps during its northward propagation. They occur in the third pentad of June, the second and fifth pentad of July, respectively. The relevant stages of the rain stagnations associated with these three jumps are defined as the South China-, Yangtze River-, and Hui River-Mei-Yu, and rainy season of North China. This classification of EASM is somewhat different from the common view of EASM life cycle at separating the traditional Mei-Yu into Yangtze River- and Huaihe River Mei-Yu. It is caused by the fact that the second jump in this study is only significant at the newly defined NPI propagations.

The interdecadal variability is evident during the progressing processes of EASM. EASM before late 1970s advances northwards quickly, reaches distance farther than its normal position, and has a longer duration in North China. As a result, above normal summer rainfall in East China occurred before late 1970s, especially for the South China Mei-Yu, Huaihe-River Mei-Yu, and the North China rainy season. In contrast, EASM after late 1970s advances northward slowly and reaches a shorter distance than its normal position. Precipitation over the majority areas in East China is below normal, except over the Yangtze River basin.

Results also demonstrate that the movement of the EASM northern edge is associated with variations of EASM intensity. Since the SMI variability can be applied to show the variations of EASM intensity, there are significant negative correlation coefficients between SMI and ENP and between SMI and ENI at interdecadal timescales. For example, ENP is located at the southern side of its climate position, when EASM is relatively weak after mid-1960s. ENP is located further south and ENI is weaker, when EASM becomes even weaker from late 1970s. ENP and ENI have a better relationship at interdecadal timescales than at interannual timescale. The differences between relationships among SMI, ENP, and ENI at interannual and interdecadal timescales suggest that interdecadal variations of the EASM northward propagation is more closely associated with the interdecadal variability of broader air–sea systems.

The northern Pacific sea-surface temperature has a prominent Pacific Decadal Oscillation (PDO) at period of 15–25 years (Latif and Barnett 1996; Zhang and Liu 1999). The PDO shows an obvious interdecadal shift in the middle of 1970s presented with a considerably large cooling over the central North Pacific Ocean. Recent studies demonstrate a significant relationship between climate variations in China and PDO (e.g., Yang et al. 2002, 2004; Zhu and Yang 2003). Results show that the atmospheric circulation anomalies associated with PDO in East Asia are correlated with the climate anomalies in China. Corresponding to the cooling shift over the central North Pacific, WPSH is weakened and shifted southeastward. The 500 hPa geopotential height increases over the Mongolia and northwestern China. In addition, a significant northerly anomaly at 850 hPa prevails over China, resulting in much weak East Asian summer monsoon. This process leads to more rainfall over Yangtze River basin and less rainfall over northern China. However, what relationships between PDO and interdecadal variations of ENP, ENI, and SMI, as well their possible mechanisms, require further investigations.

The large-scale anomaly of summer precipitation in East China has a complex but good relationship with ENP and ENI at interdecadal timescales. The interdecadal variation of summer precipitation over the Yangtze River basin is significantly negatively correlated with ENI, while positively related to ENI in South China. The interdecadal variation of summer precipitation in North China is well positively correlated with ENP. Differences of interdecadal variability of ENP and ENI and SMI are obvious. A major interdecadal shift for ENP and SMI is in middle 1960s, while in late 1970s for ENI. However, it should be noted that the changes of ENP and SMI in middle 1960s are weak, and become more significant after middle 1970s. These features demonstrate the northward propagation of EASM is a complicate process, which requires further investigation.

Acknowledgments

The first and third author would like to thank the financial support from the National Natural Science Foundation of

China (NSFC) under grant no. 40375032. The second author is supported by the NASA Global Precipitation Measurement (GPM) project. The fourth author appreciates the support of a NSFC grant no. 40275025 and the final author thanks NSFC for its support from a grant no. 90211010.

References

Basnett TA, Parker DE (1997) Development of the Global Mean Sea Level Pressure Data Set GMSLP2. Climatic Research Technical Note No. 79. Hadley Centre, Meteorological Office, Bracknell, 16 pp (plus Appendices)

Bolton D (1980) The computation of equivalent potential temperature. Mon Wea Rev 108: 1046–53

Chang CP, Zhang Y, Li T (2000a) Interannual and interdecadal variations of the East Asian summer monsoon and tropical Pacific SSTs. Part I: Roles of the subtropical ridge. J Climate 13: 4310–25

Chang CP, Zhang Y, Li T (2000b) Interannual and interdecadal variations of the East Asian summer monsoon and tropical Pacific SSTs. Part II: Meridional structure of the monsoon. J Climate 13: 4326–40

Chen LX, Zhu W, Wang W (1998) Studies on climate change in China in recent 45 year. Acta Meteor Sin 12: 1–17

Chen LX, Li W, Zhao P, Tao SY (2001) On the process of summer monsoon onset over East Asia. Acta Meteor Sin 15: 436–49

Chen LX, Zhou X, Li W, Luo Y, Zhu W (2004) Characteristics of the climatic change and its formation mechanism in China in the last 80 year. Acta Meteor Sin 62: 634–46

Chen T-C, van Loon H, Wu K-D, Yen M-C (1992) Changes in the atmospheric circulations over the North Pacific–North America area since 1950. J Meteor Soc Japan 70: 1137–46

Chen T-C, Chen JM, Wikle CK (1996) Interdecadal variation in US Pacific coast precipitation over the past four decades. Bull Amer Meteor Soc 11: 1197–205

Chen TJ (1994) Large-scale circulations associated with the east Asian summer monsoon and the Mei-Yu over South China and Taiwan. J Meteor Soc Japan 72: 959–83

Cressman GP (1959) An operational objective analysis system. Mon Wea Rev 87: 367–74

Dethof F, Dragosavac A, Fisher M, Fuentes M, Hagemann S, Hólm E, Hoskins BJ, Isaksen L, Janssen P, Jenne R, McNally AP, Mahfouf J-F, Morcrette J-J, Rayner NA, Saunders RW, Simon P, Sterl A, Trenberth KE, Untch A, Vasiljevic D, Viterbo P, Woollen J (2005) The ERA-40 reanalysis. Quart J R Meteorol Soc 131: 2961–3012

Ding YH (1992) Summer monsoon rainfalls in China. J Meteor Soc Japan 70: 373–96

Ding YH (1994) Monsoon over China. Kluwer Academic Publishers, 420 pp

Ding YH (2007) The variability of the Asian summer monsoon. J Meteor Soc Japan 85B: 21–54

Ding YH, Liu YJ (2001) Onset and the evolution of the summer monsoon over the South China during SCSMEX field experiment in 1998. J Meteor Soc Japan 79: 255–76

Ding YH, Li CY, He JH, Chen LX, Gan ZJ, Qian YF, Yan JY, Wang DX, Shi P (2004) South China Sea Monsoon experiment (SCSMEX) and the East Asian Monsoon. Acta Meteor Sin 62: 561–85

Fasullo J, Webster PJ (2003) A hydrological definition of Indian monsoon onset and withdrawal. J Climate 16: 3200–11

Gao YX, Xu SY (1962) Advances and retreats of the east Asian monsoon and the beginning and the end of rainning season – several issues of the East Asian monsoon. Science Press, Beijing, 103 pp

Gemmer M, Becker S, Jiang T (2004) Observed monthly precipitation trends in China 1951–2002. Theor Appl Climatol 77: 39–45

Gong D-Y, Wang S-W (2000) Severe summer rainfall in China associated with enhanced global warming. Clim Res 16: 51–9

Guo QY, Wang XQ (1981) Rainfall distributions of summer monsoon over China in recent 30 years. Acta Geogr Sin 36: 187–95

Hsu H-H, Terng C-T, Chen C-T (1999) Evolution of large-scale circulation and heating during the first transition of Asian summer monsoon. J Climate 12: 793–810

Jiang ZH, Chen GTJ, Wu MC (2003) Large-scale circulations patterns associated with spring heavy rain events over Taiwan in strong ENSO and non-ENSO years. Mon Wea Rev 131: 1769–82

Kalnay E, Kanamitsu M, Kistler R, Collins W, Deaven D, Gandin L, Iredell M, Saha S, White G, Woollen J, Zhu Y, Leetmaa A, Reynolds B, Chelliah M, Ebisuzaki W, Higgins W, Janowiak J, Mo KC, Ropelewski C, Wang J, Jenne R, Joseph D (1996) The NCEP/NCAR 40-year reanalysis project. Bull Amer Meteor Soc 11: 431–11

Kinter III JL, Fennessy MJ, Krishnamurthy V, Marx L (2004) An evaluation of the apparent interdecadal shift in the tropical divergent circulation in the NCEP-NCAR reanalysis. J Climate 17: 349–61

Krishnamurthy V, Goswami BN (2000) Indian monsoon-ENSO relationship on interdecadal timescale. J Climate 13: 579–95

Kumar JR, Dash SK (2001) Interdecadal variations of characteristics of monsoon disturbances and their epochal relationship with rainfall and other tropical features. Int J Climatol 21: 759–71

Lau K-M, Yang S (1997) Climatology and interannual variability of the Southeast Asian summer monsoon. Adv Atmos Sci 14: 141–62

Latif M, Barnett TP (1996) Decadal climate variability over the North Pacific and North America: dynamics and predictability. J Climate 9: 2407–23

Li CY, Zhu JH, Sun ZB (2002) The study on interdecadal climate variation. Climatic Environ Res 7: 209–19

Lian Y, Shen BC, Gao ZT, An G, Xiao XL (2003) The criteria, onset, and characteristics of East Asian summer monsoon establishment in Northeast China. Acta Meteor Sin 61: 548–58

Liao XS, Zhao ZG (1992) Seasonal prediction of summer rainfall distribution over east China. Appl Meteor 3: 1–9

Lin P-H, Lin H (1997) The Asian summer monsoon and Mei-Yu front. Part I: Cloud patterns as a monsoon index. Atmos Sci 25: 267–87

Lin ZG (1987) Advance and retreat regulations of the summer monsoon rain belt in East China. Collection of papers on meteorological science and technology. China Meteorological Press, Beijing, 24–31

Morlet J (1983) Sampling theory and wave propagation. Issues in Acoustic Signal/Image Processing and Recognition. In: Chen CH (ed) NATO ASI Series, Vol. 1. Springer, pp. 233–261

Newman M, Sardeshmukh PD, Bergman JW (2000) An Assessment of the NCEP, NASA, and ECMWF reanalyses over the tropical west Pacific warm pool. Bull Amer Meteor Soc 81: 41–7

Qian W, Yang S (2000) Onset of the regional monsoon over Southeast Asia. Meteor Atmos Phys 75: 29–38

Shi N, Zhu QG, Wang ZG (1996) The connection of summer large-scale weather-climate anomaly in China to the East Asia summer monsoon in last 40 years. Atmos Sci 20: 575–83

Sun XR, Chen LX, He JH (2004) Index of land-sea thermal difference and its relation to interannual variation of summer circulation and rainfall over east Asia. Acta Meteor Sin 60: 164–70

Tang MM, Huang SS (1983) The advance and retreat of the 1979 summer monsoon in East China. Proc. Symp. on the Summer Monsoon in Southeast Asia. People's Press of Yunnan Province, Kunming, China, pp. 15–28

Tao SY, Chen LX (1987) A review of recent research on the East Asian summer monsoon in China. In: Chang CP, Krishnamurti TN (eds) Monsoon meteorology. Oxford University Press, Oxford, pp. 60–92

Tao SY, Zhao YJ, Chen XM (1958) Mei-Yu in China. Collected Meteorological Papers of China Meteorological Administration

Teng HY, Wang B (2003) Interannual variations of the boreal summer intraseasonal oscillation in the Asia-Pacific region. J Climate 16: 3572–84

Torrence C, Compo GP (1998) A practical guide to wavelet analysis. Bull Amer Meteor Soc 79: 61–78

Trenberth KE (1990) Recent observed interdecadal climate changes in the Northern Hemisphere. Bull Amer Meteor Soc 71: 988–93

Trenberth KE, Hurrel JW (1994) Decadal atmosphere-ocean variations in the Pacific. Climate Dyn 9: 303–19

Trenberth KE, Guillemot CJ (1998) Evaluation of the atmospheric moisture and hydrological cycle in the NCEP/NACR reanalyses. Clim Dyn 14: 213–31

Tu CW, Huang SS (1944) The advances and retreats of the summer monsoon in China. Acta Meteor Sin 18: 1–20

Wang B, Fan Z (1999) Choice of South Asian summer monsoon indices. Bull Amer Meteor Soc 80: 629–38

Wang B, Wu R (1997) Peculiar temporal structure of the South China Sea summer monsoon. Adv Atmos Sci 14: 177–94

Wang B, LinHo (2002) Rainy season of the Asia-Pacific summer Monsoon. J Climate 15: 386–98

Wang B, LinHo, Zhang YS, Lu MM (2004) Definition of South China Sea monsoon onset and commencement of the East Asia summer monsoon. J Climate 17: 699–710

Wang Y, Zhou L (2005) Observed trends in extreme precipitation events in China during 1961–2001 and the associated changes in large-scale circulation. Geophys Res Lett 32: L0970; DOI: 10.1029/2005GL022574

Webster PJ, Magana VO, Palmer TN, Shukla J, Tomas RA, Yanai M, Yasunari T (1998) Monsoon: processes predictability and the prospects for prediction. J Geophys Res 103: 14451–510

Wu GX, Chou JF, Liu YM, He JH (2002) Dynamical the formation and variation of subtropical high. Science Press, Beijing, 314 pp

Wu R, Kinter JL III, Kirtman BP (2005) Discrepancy of interdecadal changes in the Asian region among the NCEP-NCAR reanalysis, objective analyses, and observations. J Climate 18: 3048–67

Yang X, Yanjuan G, Guiyu X, Xuejuan R (2002) A comparison of spatio-temporal structures between interannual and interdecadal variabilities. J Nanjing Univ 38(3): 308–17

Yang X, Yimin Z, Qian X, Xuejuan R, Guiyu X (2004) Advances in Studies of the Pacific Decadal Oscillation. Acta Atmos Sin 28(6): 979–92

Yumoto M, Mastsuura T (2001) Interdecadal variability of tropical cyclone activity in the western North Pacific. J Meteor Soc Japan 79: 23–35

Zhai P-M, Ren F-M, Zhang Q (1999) Detection of trends in China's precipitation extremes. Acta Meteor Sin 57: 208–16

Zhang RH, Liu ZY (1999) Decadal thermocline variability in the North Pacific Ocean: two pathways around the subtropical gyre. J Climate 12: 3273–96

Zheng DW, Dong DN (1986) Realization of narrow band filtering of the polar motion data with multi-stage filter. Acta Astronom Sin 27: 369–76

Zhu QG, Yang S (1989) The northward advance and oscillation of the East Asian summer monsoon. J Nanjing Inst Meteor 12: 223–30

Zhu Y, Yang X (2003) Relationships between Pacific Decadal Oscillation (PDO) and climate variability in China. Acta Meteor Sin 61(6): 641–54